Electronic Supplementary Material (ESI) for Journal of Materials Chemistry A.

Electronic Supplementary Information

Nanostructure-induced Color TiO_2 Array Photoelectrode with Full Solar Spectrum Harvesting

Chunlei Liu, Wei Zhou,* Jiakun Song, Huijuan Liu,* Jiuhui Qu, Lin Guo, Guofeng Song and Chin-Pao, Huang

S1. Experimental.

Materials and Chemicals. $Ni(ClO_4)_2\cdot 6H_2O$, $NaClO_4$, Na_2EDTA were purchased from Afla Aesar (ACS reagent). Ni(II)-EDTA solution was prepared by mixing equal molar ratio of $Ni(ClO_4)_2\cdot 6H_2O$ and Na_2EDTA. Other regents of analytical grade were obtained from Beijing Chemical Company (P.R. China) and used without further purification. Ultrapure water (18.2 $M\Omega\cdot cm^{-1}$) from a Milli-Q Plus system (Millipore) was used for the preparation, washing, and dilution.

Preparation of color TiO_2 arrays grown on Ti foams. Commercial Ti foam (purity >99.5 %), containing 99.79 % Ti, 0.01 % C, 0.17 % O, and 0.03 % H was cut into pieces with size of 2 cm × 4 cm × 1 mm (width × length × thickness) and used as electrodes or substrates to grow TiO_2. These Ti foam sheets were ultrasonically cleaned in the mixture of ultrapure water, acetone and ethanol (volume ratio of 1:1:1) for 1h and then dried for further use. In a typical synthesis, the dried Ti foam was placed against the inner wall of 50-mL Teflon-lined stainless steel autoclave filled with 30 mL of NaOH aqueous solution (4 $mol\cdot L^{-1}$). The sealed autoclaves were kept in an oven preheated to 180 °C for 4~24h and cooled to room temperature naturally. The obtained precursor of $Na_2Ti_3O_7$ on Ti foam sheets was rinsed with ultrapure water several times and then immersed in 1 $mol\cdot L^{-1}$ HNO_3 solution for 24 h to replace Na^+ with H^+. The synthesized $H_2Ti_3O_7$ nanosheet arrays were then washed, dried, and transferred into a furnace and treated at 450 °C for 1h at a ramping rate of 10 °C min^{-1} in air. The TiO_2 arrays grown on Ti foam sheets with different color were prepared. The red TiO_2 array grown on Ti foam (R-TiO_2/TF), the purple one (P-TiO_2/TF), the blue one (B-TiO_2/TF), the green one (G-TiO_2/TF), and the white one (W-TiO_2/TF) were corresponding to the precursor of $Na_2Ti_3O_7$ annealed at 180°C for 4h, 6h, 8h, 12h and 24h, respectively. The P25/Ti foam electrode was made by depositing commercial P25 powder on the Ti foam using a dip-coating technique. [S1] The mass of deposited P25 powder was 0.056 g, which was equal to the red TiO_2.

Preparation of the TiO_2 powder with mixed phases. According to the reference [S2], in a typical process, 2.25 g of anatase powder was mixed with 30 mL of 10 $mol\cdot L^{-1}$ NaOH. The suspensions were sonicated in an ultrasonic bath for 30 min and then transferred into a PTFE autoclave. The autoclave was maintained at 180 °C for 48h. The precipitate was washed with ultrapure water, immersed in 0.1 $mol\cdot L^{-1}$ HCl solution to produce $H_2Ti_3O_7$, and washed again with ultrapure water until pH ~ 7 was reached. The products were dried at 80°C and dispersed in an autoclave with 0.05 $mol\cdot L^{-1}$ HNO_3 (40 mL) autoclaved at 110 °C for 8 h. After washing and drying, the precursor turned into product with mixed phases of anatase and TiO_2(B) after heating at 450 °C for 1 h.

Characterization. The X-ray diffraction spectrum (XRD) was obtained by X'Pert PRO MPD with Cu K_α radiation over the 2θ range of 10-90°. The morphology and structure of the TiO_2 arrays were characterized by field-emission scanning electron microscopy (FE-SEM, SU8020, HITACHI), transmission electron microscopy (TEM), and high-resolution TEM (HRTEM, JEM-2100, JEOL, Japan). The chemical state and the component of the photoanode were investigated by X-ray photoelectron spectra (XPS, PHI-5300/ESCA, ULVAC-PHI, INC). All binding energies were calibrated by using contaminant carbon (C 1s = 284.8 eV) as a reference. UV-Vis-NIR absorption spectra of the samples were measured using a UV-vis-NIR diffuse reflectance spectrophotometer (Cary 5000, Varian) equipped with an integrating sphere at room temperature. Raman spectra were carried out with a confocal Raman spectroscopy system (Renishaw Invia Raman microscope) equipped with a Leica microscope with 10, 50, 100× objectives and a 532 nm laser lines as the excitation source.

Photoelectrochemical (PEC) measurements. All the measurements were carried out with an electrochemical workstation (Gamry, Interface1000, USA) in a standard three-electrode quartz cell. The color TiO_2 grown on Ti foam (TiO_2/TF), a saturated calomel electrode (SCE), and platinum wire were used as the photoanode (the working electrode), counter electrode, and reference electrode, respectively. The solution containing 0.1 $mol \cdot L^{-1}$ Na_2SO_4 was used as the supporting electrolyte. A Xeon lamp (Beijing Aulight Co. Ltd, China; wavelength, 200-780 nm, 20A) was used as the simulated sunlight source. The irradiation distance from the light source to the TiO_2 sheet was set as 8 cm. The electrochemical impedance spectroscopy (EIS) was carried out at 0 V vs SCE in the frequency range of 0.01 Hz-100 kHz with AC voltage of 10 mV. The used area of the TiO_2 photoanode was 5 cm^2. The transient response of photocurrent was collected as switching the light on and off every 30 seconds at the applied potential of 0.5 V vs SCE under simulated sunlight illumination.

S2. Degradation of selected chemical species by color TiO_2/TF anodes.

PEC degradation of Ni(II)-EDTA. All degradation experiments were carried out at room temperature in a three-electrode single-compartment quartz cell. The applied area of the TiO_2/TF was set as 5 cm^2, a Ti foil with the same area was used as the counter electrode, and a SCE as the reference electrode. The distance between the electrodes was 1.5 cm and a constant current density of 0.6 $mA\cdot cm^{-2}$ (corresponding applied voltage of 1.0 V by R-TiO_2/TF with PEC method, 3.0 V by bare Ti Foam with EC method). A Xeon lamp was used as the light source. Ionic strength was prepared in 10 $mmol\cdot L^{-1}$ of $NaClO_4$ with pH adjusted to ~3.5. 70 mL of Ni(II)-EDTA solution (e.g., 0.05, 0.1, 0.25, and 0.5 $mmol\cdot L^{-1}$) was separately placed in the reaction cell under the simulated sunlight. The distance between the light source and the photoanode was set as 8 cm. The Ni(II)-EDTA concentration was determined using a high performance liquid chromatography (HPLC, 1260, Agilent Technology) equipped with a C-18 column (Agilent Technology) and two detectors connected in series, namely, a diode array detector (Waters 996) and a fluorescence detector (Waters 474). Concentration of total Ni in the solution was measured using a 710 series inductively coupled plasma optical emission spectrometer (ICP-OES, Agilent Technology, USA). The Ni(II)-EDTA removal efficiency and the Ni^{2+} recovery efficiency were calculated according to the following equation:

$$R = (C_0-C_t) / C_0 \qquad (1)$$

where R is the Ni(II)-EDTA removal efficiency or the Ni^{2+} recovery efficiency，C_0 is the initial Ni(II)-EDTA concentration (obtained by HPLC) or total Ni in the solution (obtained by ICP), and C_t is the concentration of Ni(II)-EDTA or total Ni in the solution over a period of time. The intermediates including formic acid, acetic acid, and inorganic ions such as NO_3^- were identified by a Dionex 2000 ion chromatograph (IC), equipped with an IonPac AS-19 anion-exchange analytical column and an IonPac AG19 guard column. KOH solution was used for mobile phase eluent. The intermediates were obtained under gradient elution conditions (0.0-30.0 min, 10.0 $mmol\cdot L^{-1}$ KOH, flow rate: 1.0 $mL\cdot min^{-1}$) with injection volume of 25 μL each time.

Photocatalytic degradation of methyl orange. The photocatalytic degradation of methyl orange aqua-solution (MO, $C_{14}H_{14}N_3NaO_3S$, 15 $mg\cdot L^{-1}$×70 mL) was used to study the long-term stability of R-TiO_2/TF electrode at pH ~4.6. 1 mL of the mixture was taken every 30 min for analysis. The MO concentration was determined by the absorbing intensity at 463 nm (main absorption peak of MO) using UV-Vis spectrometer. Before each degradation experiment, the reaction solution was continuously stirred in the dark for 30 min to obtain the MO adsorption/desorption equilibrium on the TiO_2/TF electrode.

S3. Numerical simulation.

Numerical simulation of the periodically arranged wedge-like model was carried out using finite element method (FEM). Polarized plane wave was used as incident light on the wedge-like model in the UV, visible, and near-infrared region. The simplified wedge-shaped array model in FEM simulation was set on a semi-infinite substrate with periodic boundary of 350 nm (containing one wedge-like sheet) in the UV and visible region. The wedge-like array model in the near-infrared region was set with periodic boundary of 875 nm in the x-z plane and 500 nm in the y-z plane. The refractive index of TiO_2 and Ti used in the simulation was 2.5 and 2.15, respectively [S3, S4].

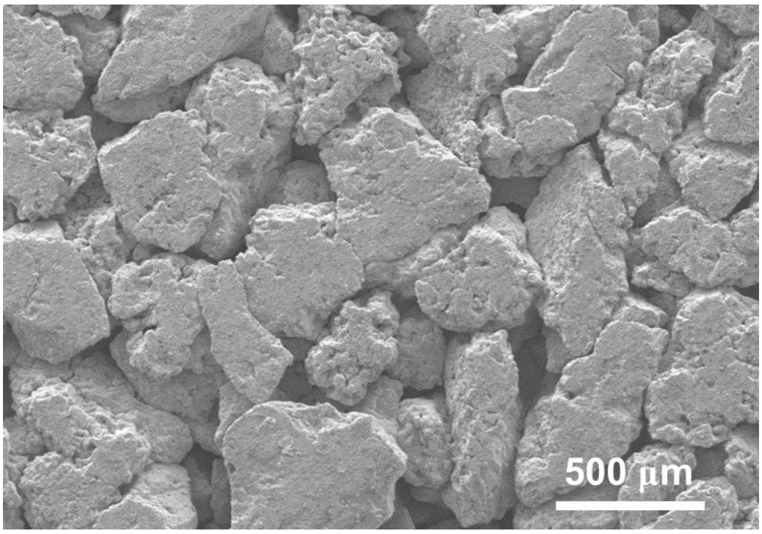

Fig. S1. SEM image of Ti foam composed of particles with sizes of 200~500 μm.

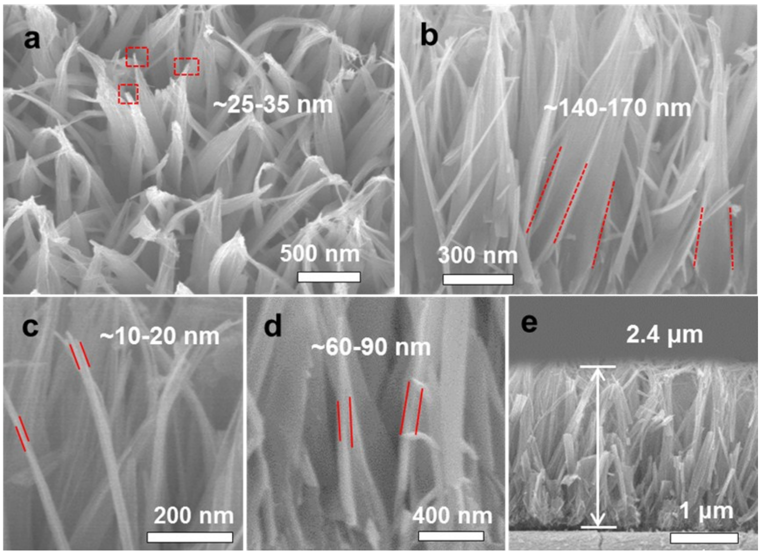

Fig. S2. Size of tip width (a), end width (b), tip thickness (c), end thickness (d), and length (e) of the R-TiO_2/TF sample from SEM images.

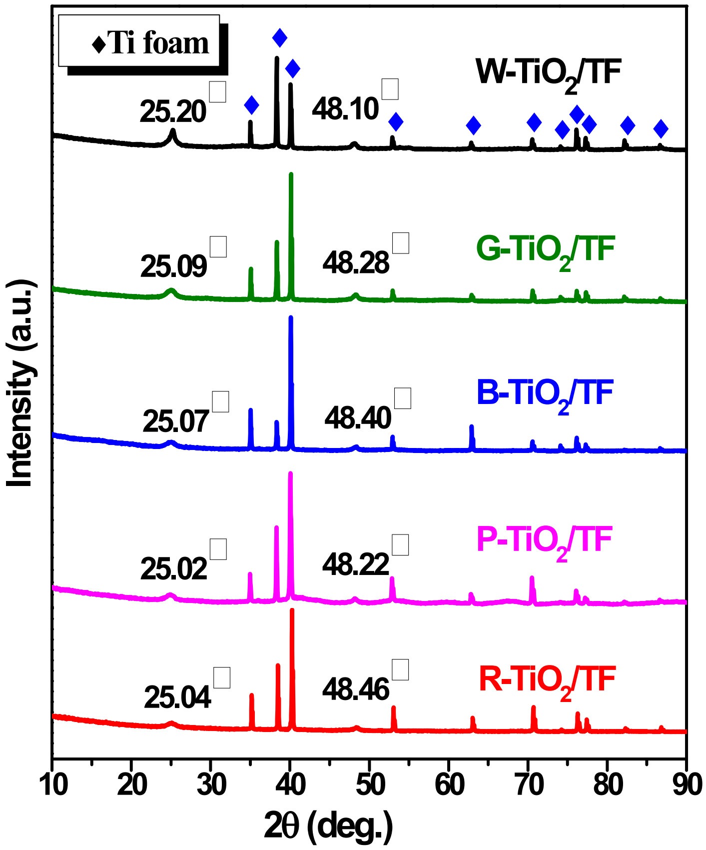

Fig. S3. XRD patterns of the five color TiO_2/TF electrodes. The peaks marked with diamonds could be ascribed to the component of Ti foam (JCPDS No. 44-1294). According to the two characteristic peaks of TiO_2(B) at 24.90° and 48.50° (JCPDS No. 46-1238) and peaks of anatase (JCPDS No. 21-1272) at 25.20° and 48.10°, we could deduce the photocatalysts of R-TiO_2, P-TiO_2, B-TiO_2, and G-TiO_2 were hybrids of two phases of anatase and TiO_2(B) as their corresponding peak values between 24.90° (48.50°) and 25.20° (48.10°), while the W-TiO_2 was consistent with anatase TiO_2.

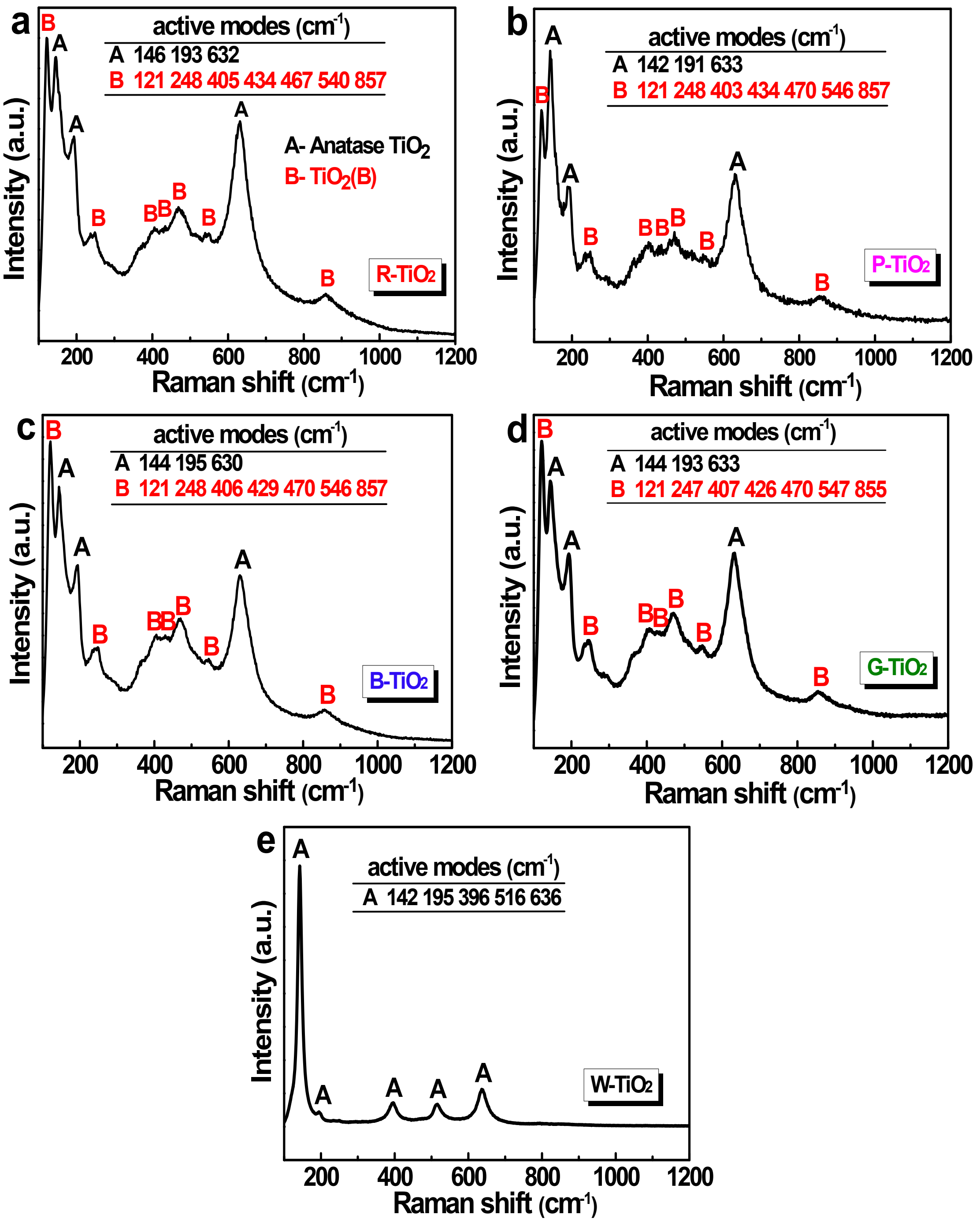

Fig. S4. Raman spectra for the photocatalysts of R-TiO_2 (a), P-TiO_2 (b), B-TiO_2 (c), G-TiO_2 (d), and W-TiO_2 (e). The phase of TiO_2(B) was marked with red and anatase with black. For anatase TiO_2, there are six Raman active modes with frequency at 144, 197, 399, 515, 519 (superimposed with the 515 cm^{-1} band), and 639 cm^{-1} [S5]. For TiO_2(B), frequency at 121, 251, 408, 430, 465, 550, and 856 cm^{-1} were active modes [S6]. The peaks above for the five photocatalysts were carefully marked and indexed to the two phases of anatase and TiO_2(B). It was obvious that R-TiO_2, P-TiO_2, B-TiO_2, and G-TiO_2 were composed of two phases whereas the W-TiO_2 was a pure anatase, which was in agreement with results of XRD analysis.

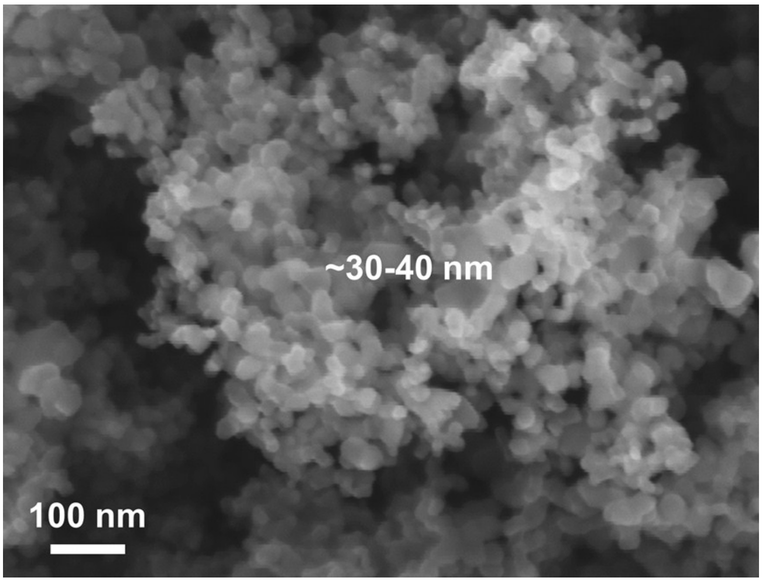

Fig. S5. SEM image of commercial P25. It was seen that the diameter of P25 particles was ~30-40 nm.

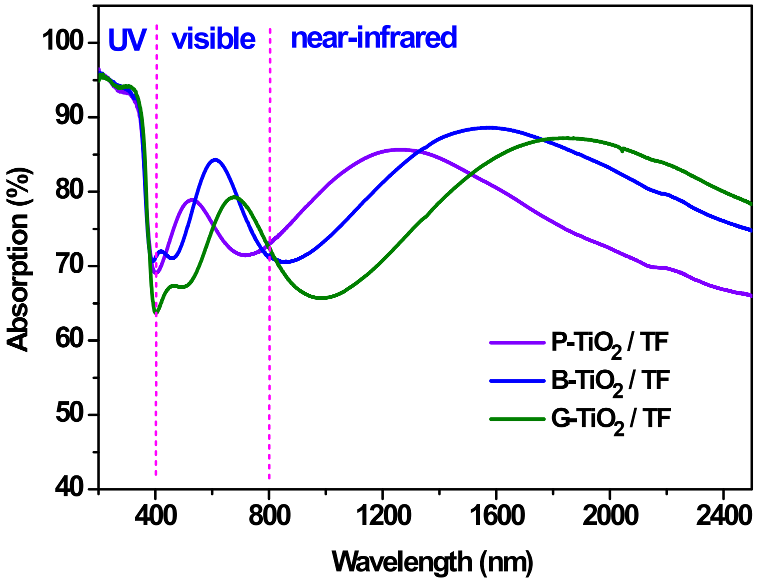

Fig. S6. UV-Vis-NIR absorption spectra of the other three samples of P-TiO_2/TF, B-TiO_2/TF and G-TiO_2/TF electrodes. Each photocatalyst had an absorption peak in the visible region corresponding to their specific color, such as 521 nm for P-TiO_2, 606 nm for B-TiO_2, and 670 nm for G-TiO_2. Additionally, we found that the color TiO_2/TF also had obvious absorption in the near-infrared region from 800 to 2500 nm, such as ~1264 nm for the P-TiO_2/TF, ~1579 nm for the B-TiO_2/TF, and ~1852 nm for the G-TiO_2/TF electrode.

Table S1. Macroscopic color and the corresponding absorption wavelength

Macroscopic color	wavelength (nm)	experimental absorption wavelength (nm)
red	**480-500**	**490**
purple	**500-580**	**521**
blue	**580-650**	**606**
green	**650-750**	**670**

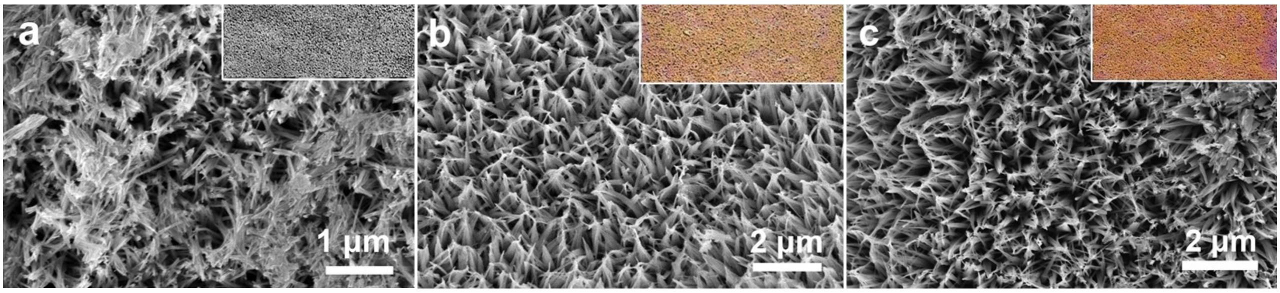

Fig. S7. SEM image for $Na_2Ti_3O_7$ (a), $H_2Ti_3O_7$ (b), and TiO_2 arrays (c) grown on Ti foam. First, precursor $Na_2Ti_3O_7$ was turned to $H_2Ti_3O_7$ upon H^+ replacement, then turned to TiO_2 arrays after calcination. The insert showed the related macroscopic color of the photocatalysts. We could deduce the relationship between the ordered array structure and the color.

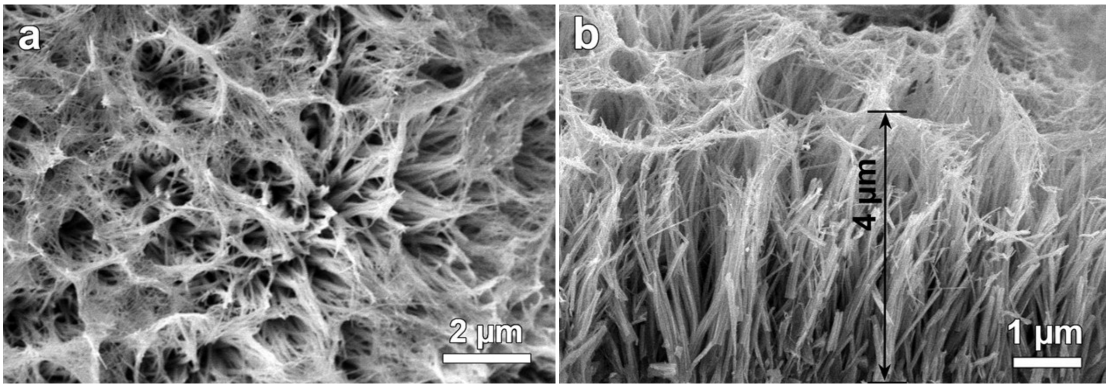

Fig. S8. SEM image of the top (a) and the side view (b) of the white sample (W-TiO_2). As the reaction time was prolonged, the TiO_2 array could grow up to ~4 μm in length. Note that there were tangled nanosheets on the top, which messed up the ordered wedge-like arrays.

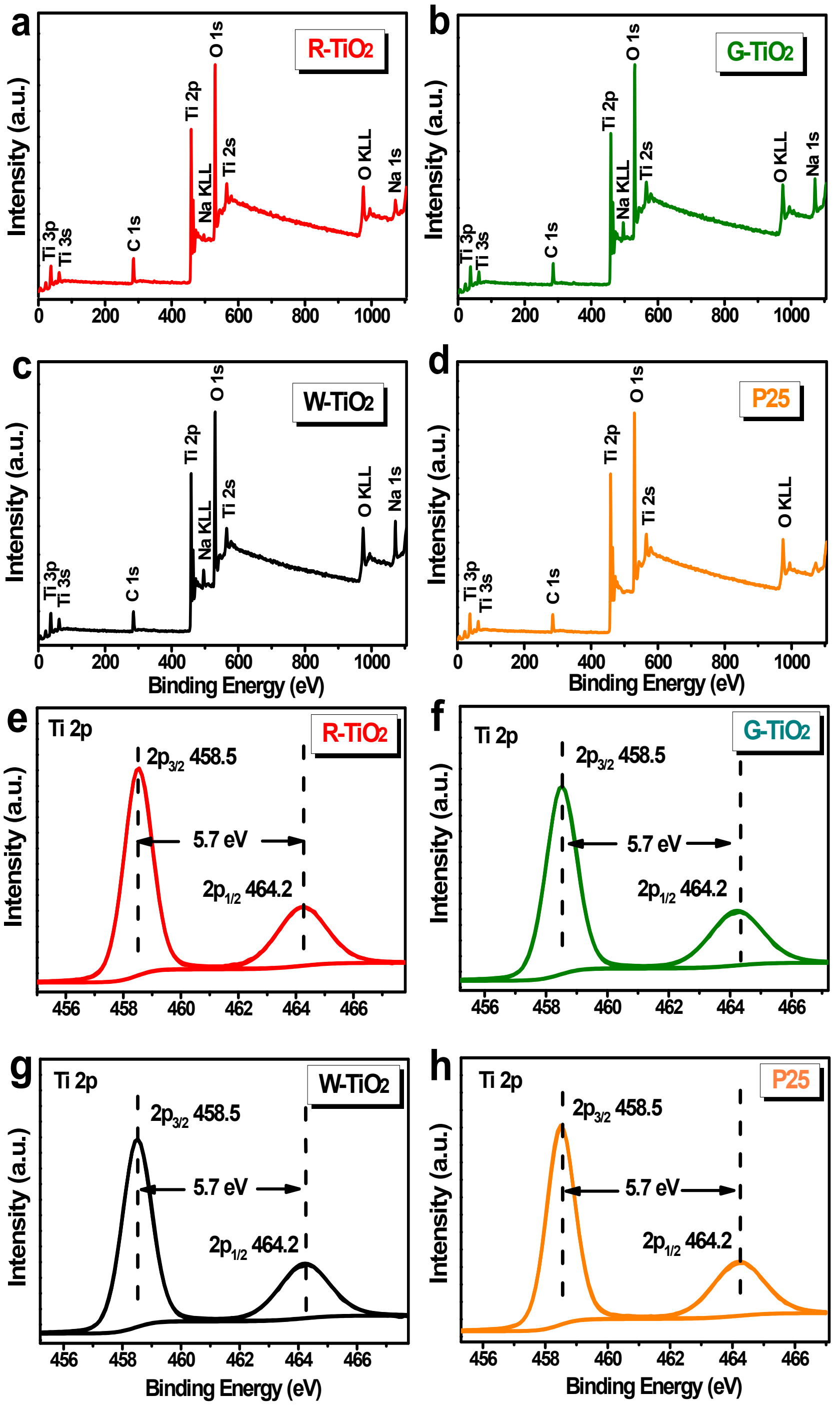

Fig. S9. The survey XPS spectra of (a) R-TiO_2, (b) G-TiO_2, (c) W-TiO_2, and (d) commercial P25. The prepared photocatalysts contained a little amounts of Na^+ residue coming from NaOH. The survey spectra also confirmed that there was no N element, which excluded the possibility color of the photocatalysts was from N doping. Ti 2p XPS spectra of (e) R-TiO_2, (f) G-TiO_2, (g) W-TiO_2, and (h) P25 further showed that the distance between Ti $2p_{3/2}$ and Ti $2p_{1/2}$ of each sample was 5.7 eV [S7-S9], confirming the normal state of Ti^{4+} instead of Ti^{3+}, indicating the color was not resulted from Ti^{3+} or O vacancies [S10, S11].

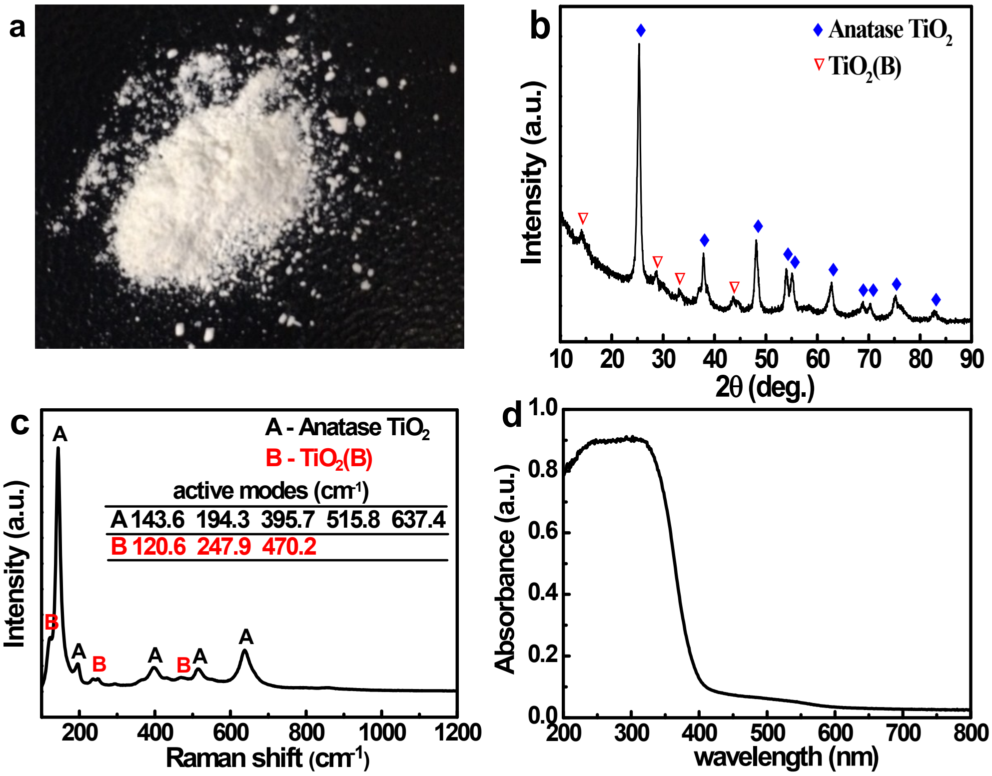

Fig. S10. (a) Photograph of white TiO_2 powder, (b) XRD pattern, (c) Raman spectra, and (d) UV-Vis spectra for synthesized TiO_2 powder composed of anatase and TiO_2(B). It gave evidence that mixed phases were not the sources of color change, as there was no absorption peak in the visible range.

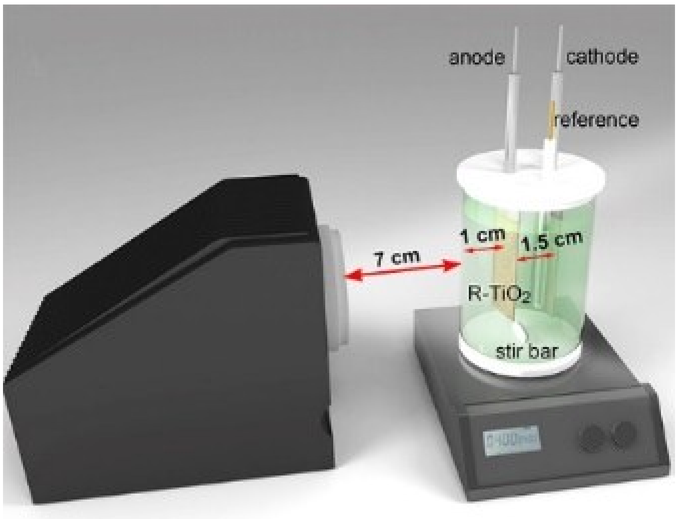

Fig. S11. Illustration of the three-electrode photoelectrochemical system. The R-TiO_2/TF, Ti foil, and Hg/$HgCl_2$ were used as the anode, cathode, and reference electrode, repectively.

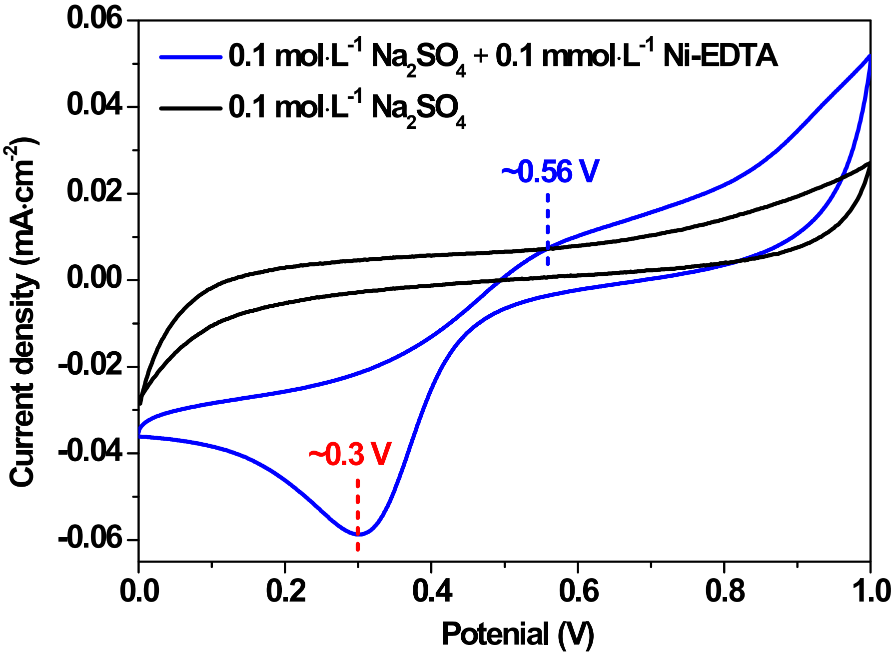

Fig. S12. Cyclic voltammetry curves of 0.1 mmol·L^{-1} Ni-EDTA in 0.1 mol·L^{-1} Na_2SO_4 solution (blue line), and in 0.1 mol·L^{-1} Na_2SO_4 solution (black line).

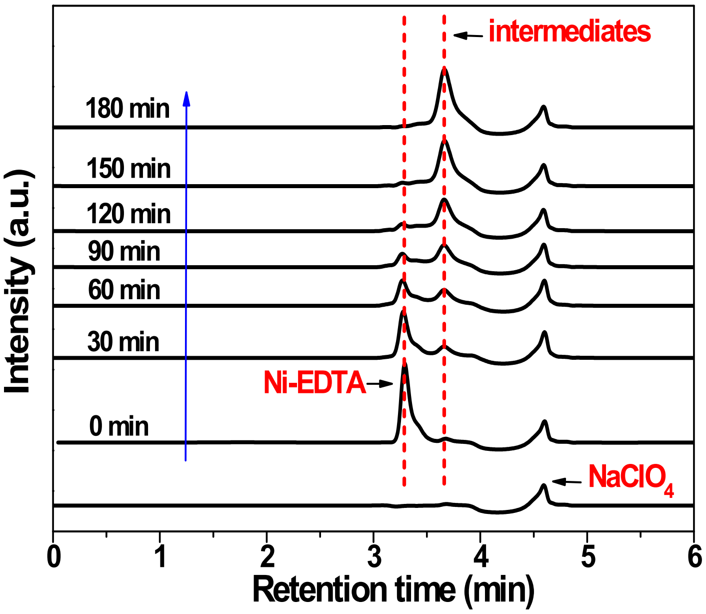

Fig. S13. Retention time of Ni(II)-EDTA solution (containing Ni(II)-EDTA and $NaClO_4$) and its intermediates with PEC degradation at different interval time (R-TiO_2/TF as photoanode). It was obvious the Ni(II)-EDTA was decreased and the intermediates were increased with time.

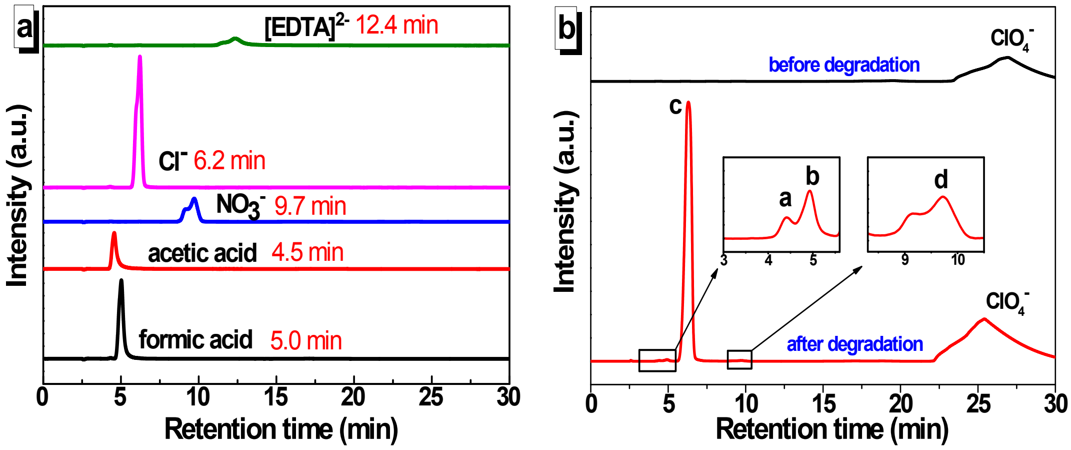

Fig. S14. (a) Retention time obtained by adding pure Na_2[EDTA], NaCl, $NaNO_3$, acetic acid, and formic acid separately. (b) Retention time of some intermediates obtained from the Ni(II)-EDTA solution (containing Ni(II)-EDTA and $NaClO_4$) before and after PEC degradation.

Table S2. Identification of intermediates from Ni(II)-EDTA after PEC degradation

Standards					
	acetic acid	**formic acid**	**Cl^-**	**NO_3^-**	**$[EDTA]^{2-}$**
Retention time (min)	4.5	5.0	6.2	9.7	12.4
Detected intermediates					
	a	**b**	**c**	**d**	
Retention time (min)	4.4	4.9	6.3	9.7	

From Fig. S13, S14, and Table S2, we could deduce that the Ni(II)-EDTA solution (containing Ni(II)-EDTA and $NaClO_4$) was decomposed to small organic acids (e.g., acetic acid and formic acid), NO_3^-, and other small molecules through decomplexation and further oxidization. Meanwhile, ClO_4^- ions were also partially decomposed to Cl^- ions. In this communication, we did not differentiate the contribution to degradation due to adsorption, decomplexation, or decomposition in the PEC process.

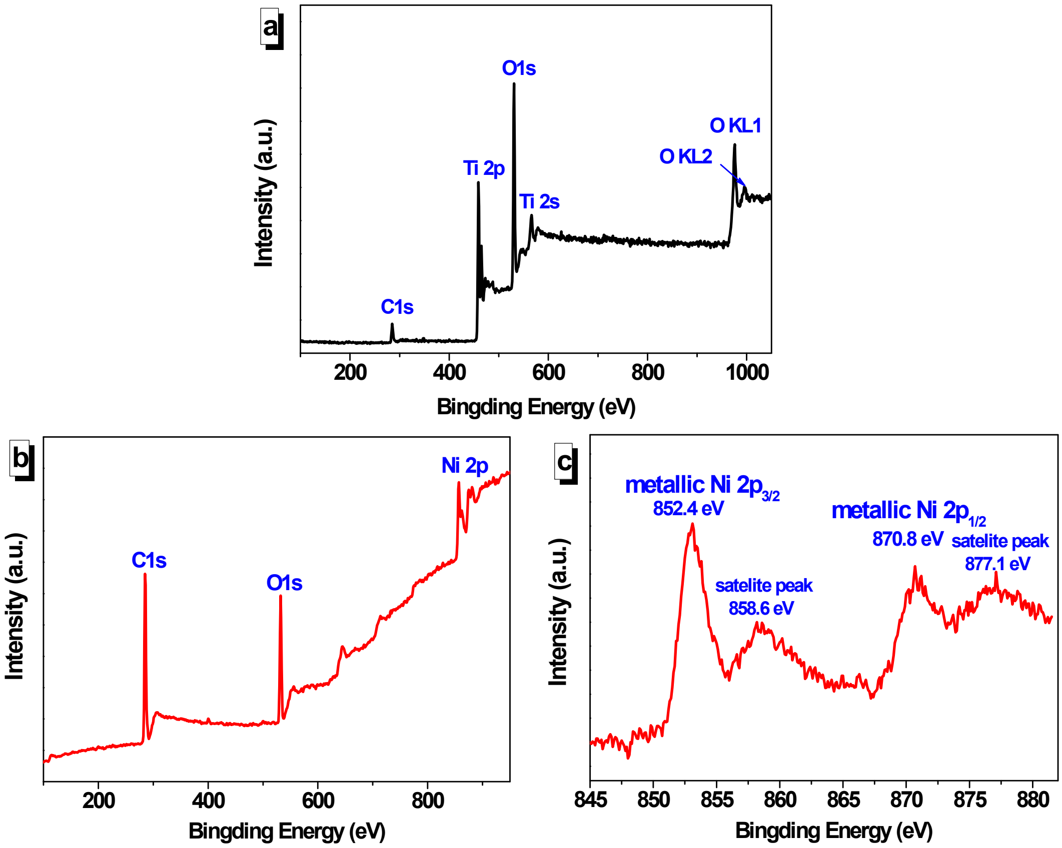

Fig. S15. The survey XPS spectra of the R-TiO_2 photoanode after degradation of Ni(II)-EDTA (a), the Ti foil cathode after degradation of Ni(II)-EDTA (b) and metallic Ni 2p XPS spectra (c) in PEC process. Results of the survey XPS spectra showed that metallic nickel was not detected at the R-TiO_2 photoanode but found at the surface of Ti foil. The strong peaks at binding energy of Ni2$p_{3/2}$ within the range of ~852-853 eV and Ni2$p_{1/2}$ of 870-871 eV were attributed to the metallic Ni [S12-S14], indicating Ni^{2+} was reduced at the surface of the Ti foil. The weak satellite peaks (858.6 eV and 877.1 eV) arising from the primary peaks of Ni 2p indicated metallic nickel deposition at the surface of Ti foil.

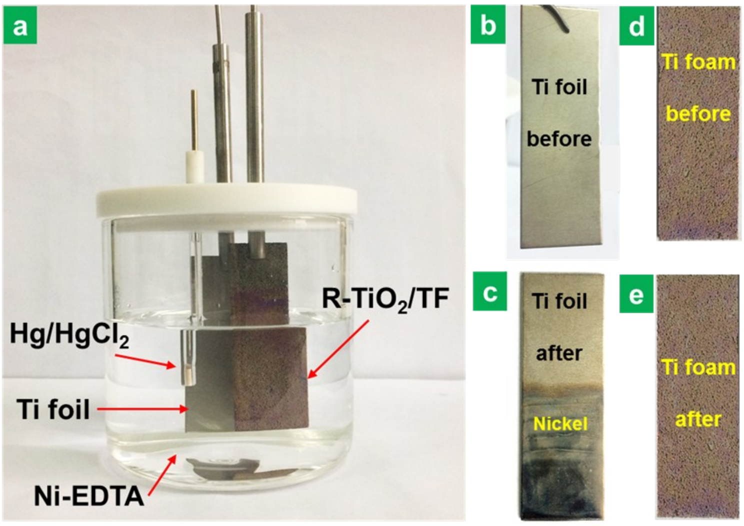

Fig. S16. Digital images of the three-electrode system (a), Ti foil cathode before (b) and after (c) nickel deposition, Ti foam photoanode before (d) and after (e) Ni(II)-EDTA degradation.

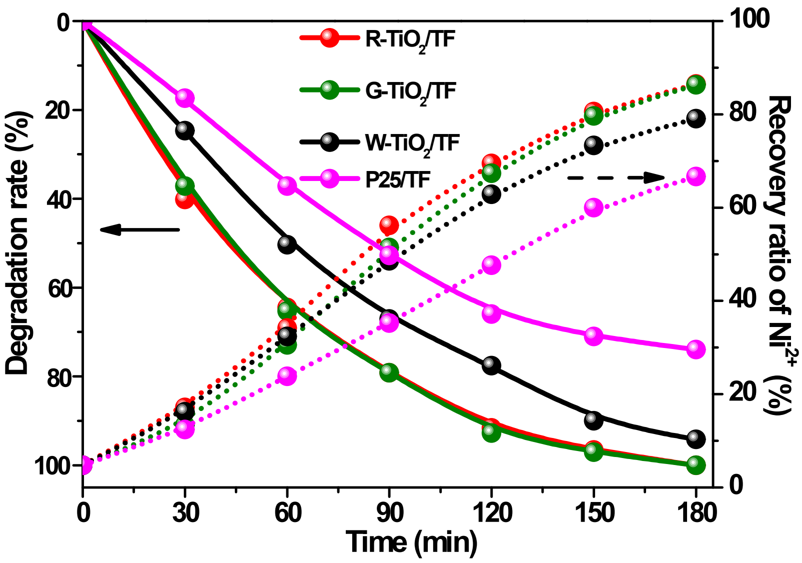

Fig. S17. Removal efficiency of Ni(II)-EDTA (solid lines, 0.05 mmol·L^{-1}) and the corresponding Ni^{2+} recovery efficiency (dotted lines) using R-TiO$_2$/TF, G-TiO$_2$/TF, W-TiO$_2$/TF and P25/TF photoanodes. The removal efficiency were 100 %, 100 %, 94 %, and 74%, and the recovery efficiency were 86 %, 86 %, 78 %, and 65% by the R-TiO$_2$/TF, G-TiO$_2$/TF, W-TiO$_2$/TF, and P25/TF electrodes, respectively.

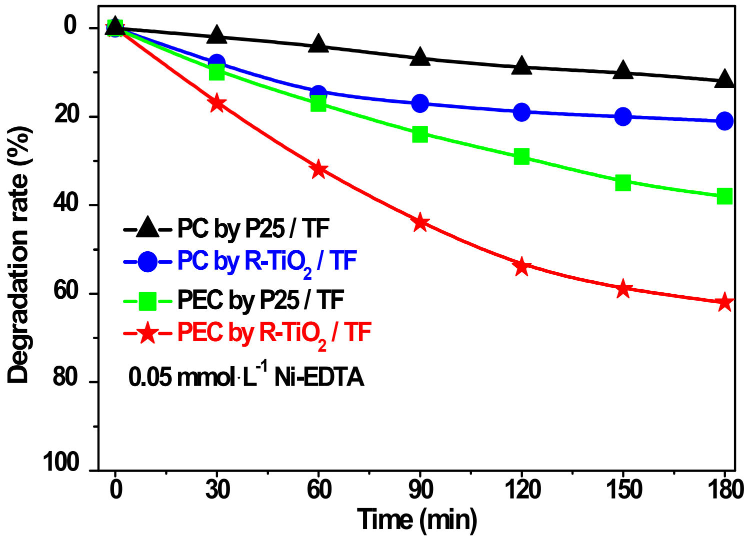

Fig. S18. The removal efficiency of Ni(II)-EDTA (0.05 mmol·L^{-1}) by R-TiO$_2$/TF and P25/TF were 62 % and 38% with PEC method, and 21 % and 12% with PC method after 180 min under visible light (λ > 400 nm).

Table S3. Comparison of energy consumption by electrochemical degradation of metal complexes

Species	**Concentration ($\mathbf{mg \cdot L^{-1}}$)**	**Energy consumption (E_c) ($\mathbf{kWh \cdot m^{-3}}$)**	**Refs**
copper cyanide	26	0.30	S15
Ni complex	20	0.60	S16
Cu complex	45	2.00	S17
Ni complex	25	4.00	S18
Ni(II)-EDTA (PEC)	40	0.08	**This work**
Ni(II)-EDTA (EC)	40	3.15	

In light of energy crisis, low electrical energy consumption ($kWh \cdot m^{-3}$) is extremely necessary criteria for applying electrochemical degradation of organic pollutants. The electrical energy consumption (E_c) in our system using R-TiO_2 electrode was calculated by Eq. 4 [S19, S20],

$$E_c = \frac{1000Pt}{60V \cdot \log(C_0 / C_t)} \qquad (4)$$

where P is the electric power of the electrochemical system (kW), V is the volume (L) of the solution in the reactor, t is the degradation time (min), C_0 is the initial concentration of the metal complex, and C_t is the concentration of metal complex over a period of time. The calculated E_c value was 0.08 $kWh \cdot m^{-3}$ for our work, compared to 0.30, 0.60, 2.00, and 4.00 $kWh \cdot m^{-3}$ reported by others and 3.15 $kWh \cdot m^{-3}$ by bare Ti foam in our work (Table S3). Our low energy consumption might be attributed to contribution from photocatalytic activity as the electric energy consumption was minute in our system, which was the original aim of this research to use sunlight to reduce power consumption.

Table S4. Photocatalytic degradation of different metal EDTA complexes

Species	**Concentration ($mmol\cdot L^{-1}$)**	**Time (h)**	**Degradation efficiency (%)**	**TiO_2 Content ($g\cdot L^{-1}$)**	**Refs**
Ni(II)-EDTA	0.13	0.5	25	2	S21
Cu(II)-EDTA	0.05	1	90	2	S22
Cu(II)-EDTA	0.1	3	100	2	S23
Cd(II)-EDTA	0.1	3	70	2	S24
Cu(II)-EDDS	0.2	4	24	0.05	S25
As(III)-EDTA	0.05	6	15	1	S26
EDTA	1	1	60	1	S27
Ni(II)-EDTA (PEC)	0.1	3	100	0.4	**this work**

The TiO_2 content of our photocatalyst was calculated by the following equation,

$$d = 0.5*(m_1-m_2)*1000/V \qquad (5)$$

where d is the catalyst content ($g\cdot L^{-1}$), m_1 is the weight of R-TiO_2/TF electrode with an area of 5 cm^2, m_2 is the weight of the same R-TiO_2/TF electrode upon immersion in the mixture of HF: HNO_3: H_2O (volume ratio of 1:4:5) until the color becomes invisible, V is the volume of Ni(II)-EDTA solution (70 mL). The calculated d value was 0.4 $g\cdot L^{-1}$. The coefficient of 0.5 was a correction for R-TiO_2 as it grew on both sides of Ti foam and we used only one side.

Our photoelectrochemical degradation using R-TiO_2/TF as photoanode had the following advantages over the powder photocatalysts. As shown in Table S5, a 100% removal efficiency of 0.1 $mmol\cdot L^{-1}$ Ni(II)-EDTA was obtained, which was much higher than those reported by others. Meanwhile, a 94% of Ni^{2+} was collected in our work but there was no Ni^{2+} recovery by only photocatalysis. Most of all, the catalyst content of our work (0.4 $g\cdot L^{-1}$) was lower than most powder catalysts. Moreover, the degradation of metal complex using R-TiO_2/TF photoanode was much easier to recover, recycle, and reuse than powder catalysts.

Table S5. Comparison of removal efficiency with photoelectrochemical degradation

Electrode	**Species**	**Concentration (mmol·L^{-1})**	**Area (cm^2)**	**Light intensity (mW/cm^2)**	**Volume (mL)**	**Time (h)**	**Degradation (%)**	**Recovery (%)**	**Refs**
Ti foil	Ni(II)-EDTA	0.05	60	1.5$^{\#}$	450	3	90	45	S28
Ti mesh	Cu(II)-EDTA	0.1	78.5	NA$^{\#}$	450	1	80	60	S29
Ti foil	Cu(II)-EDTA	0.05	35	8$^{\#}$	400	3	72	67	S30
Ti foam	Ni(II)-EDTA	0.1	5	500	70	3	100	94	**this work**

#: UV lamp (main wavelength at 254 nm)

In Table S5, we reported a total (100 %) degradation of EDTA and 94 % metal recovery using red TiO_2/TF as photoelectrode, which was much improved compared with the results with degradation efficiency of 72-90 % and metal recovery of 45-67 %. Obviously, our much enhanced Ni(II)-EDTA degradation and Ni recovery were obtained by using special photoelectrode with PEC method.

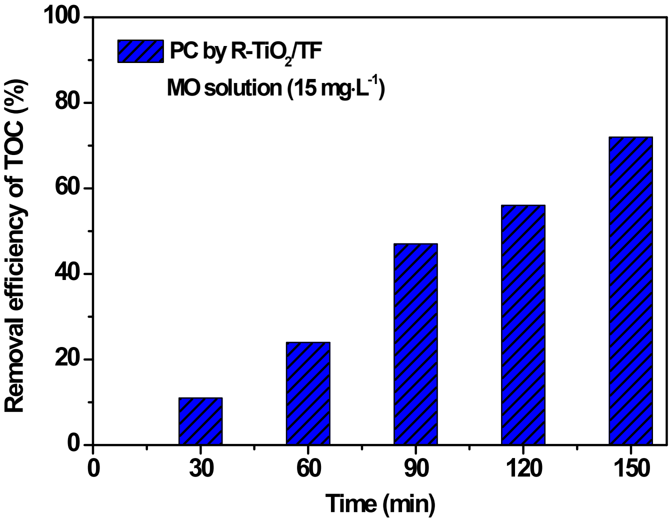

Fig. S19. Total organic carbon (TOC) of MO (15 mg·L-1) by the R-TiO_2/TF photoanode with PC method under the simulated sunlight. Results showed 72% TOC was removed after 150 min degradation.

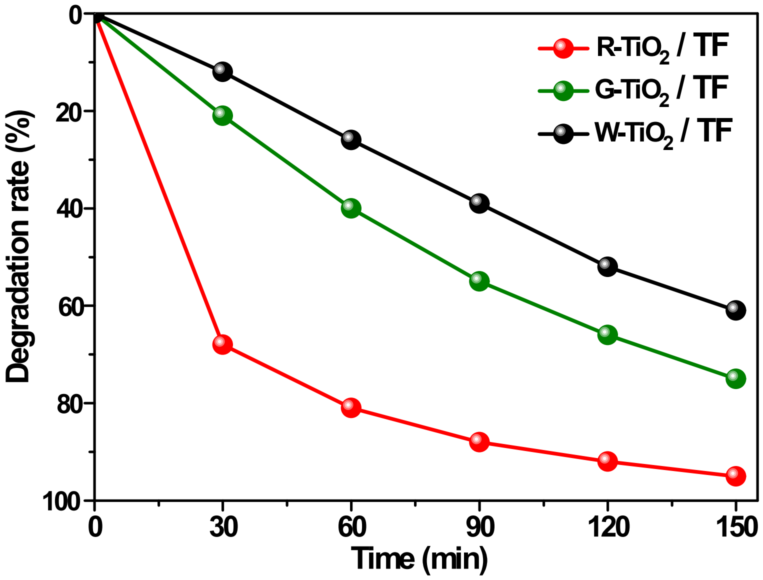

Fig. S20. The photocatalytic removal efficiency of MO (15 mg·L^{-1}) was 95 %, 75 %, and 61 % after 150 min by R-TiO$_2$/TF, G-TiO$_2$/TF, and W-TiO$_2$/TF electrodes, respectively, which clearly showed that the R-TiO$_2$/TF had the best photocatalytic reactivity towards MO molecules.

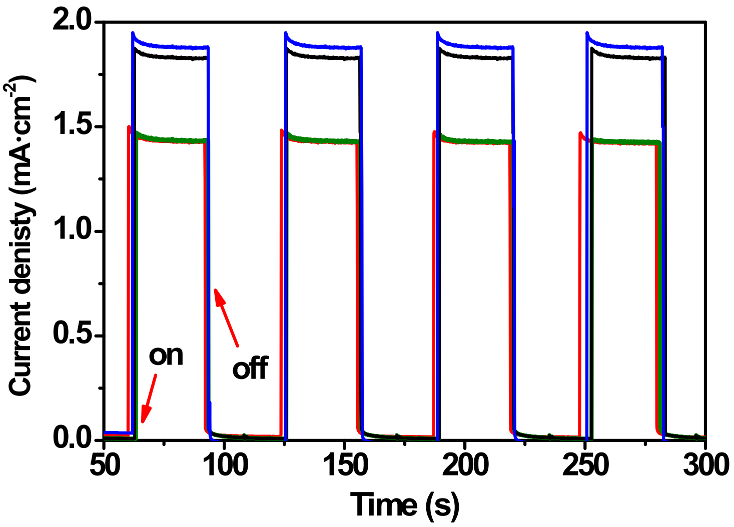

Fig. S21 Transient photocurrent response by the R-TiO$_2$/TF (red line and black line under 0.5 V and 0.8 V vs. SCE without Ni(II)-EDTA; green line and blue line with 0.1 mmol·L^{-1} Ni(II)-EDTA under 0.5 V and 0.8 V vs. SCE) in 0.1 mol·L^{-1} Na$_2$SO$_4$.

In Fig. S21, the similar trend can be observed when 0.8 V bias voltage was applied. In addition, no obvious photocurrent change under the applied bias voltage of 0.5 V could be observed which was probably due to the quantity of separated hole-electron pairs under the low voltage had not the sufficient potential to oxidize Ni(II)-EDTA with low concentration (0.1 mmol·L^{-1}) and as a result most photocurrent generated from photoelectrochemical water oxidation.

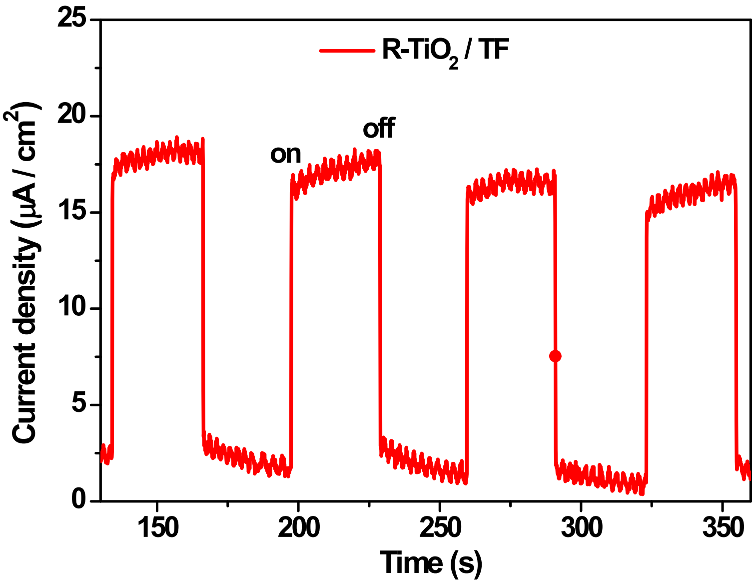

Fig. S22. Transient photocurrent response for the R-TiO$_2$/TF electrode under visible light irradiation ($\lambda >$ 400 nm).

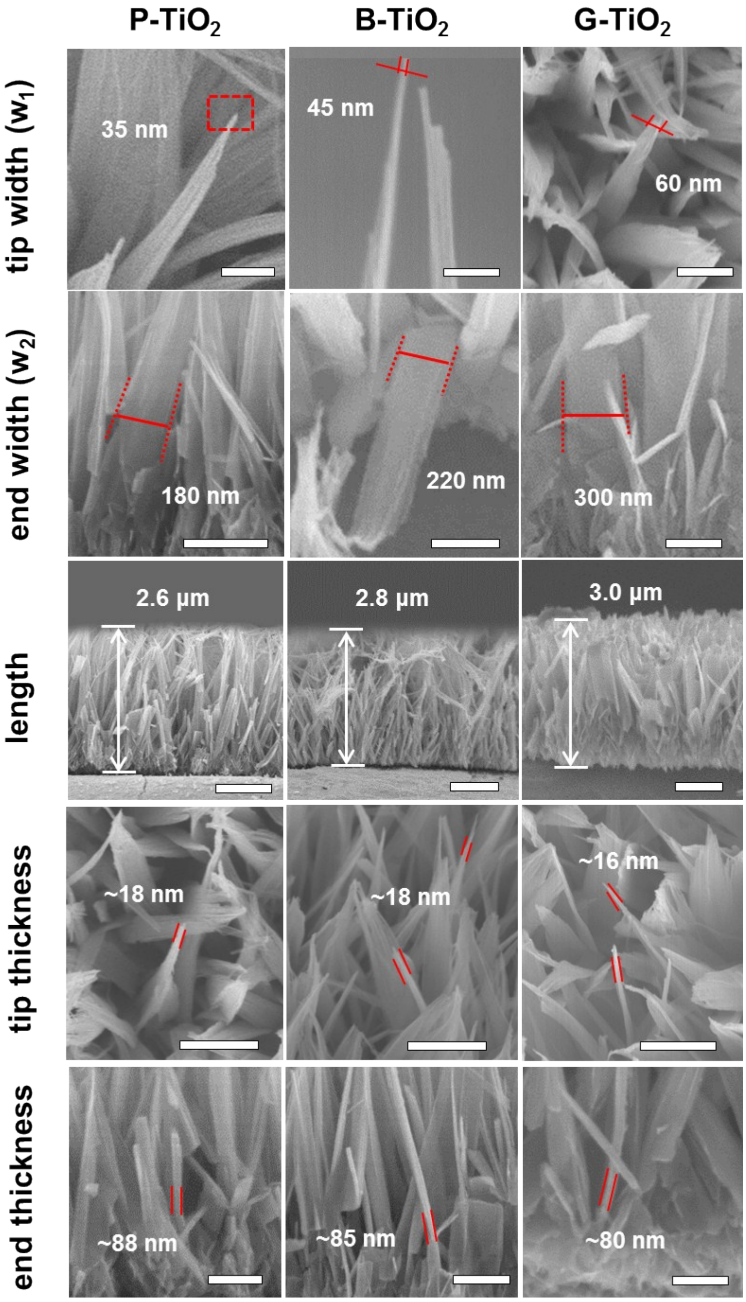

Fig. S23. SEM images of the P-TiO_2, B-TiO_2, and G-TiO_2 samples. The images showed details of the wedge-like sheets. The sizes were summarized in Table S8 and used in FEM simulation. (Scale bar: 300 nm in Lines 1 and 2, 1 μm in Line 3, 200 nm in Line 4, and 500 nm in Line 5).

Table S6. Size used as the simulation parameters taken from the SEM images of the wedge-like sheets

R-TiO_2	**UV region** **（E_y）**	**visible region** **(E_x)**	**near-infrared region** **(E_x)**
width (top, W_1)	**25-35 nm**	**25-35 nm**	**100-120 nm**
width (bottom, W_2)	**140-170 nm**	**140-170 nm**	**500-550 nm**
Length (L)	**2.4 μm**	**2.4 μm**	**2.4 μm**
thickness (top, T_1)	**10-20 nm**	**10-20 nm**	**20-30 nm**
thickness (bottom, T_2)	**60-90 nm**	**60-90 nm**	**90-100 nm**

The near-infrared absorption might be influenced by bigger size as the increased wavelength in NIR region compared to UV and visible light. The bigger sizes of the five parameters for NIR could be ascribed to the aggregated sheets (as shown in Fig. S22).

Table S7. UV absorption at 300 nm by TiO_2 before and after modification

	after	before	after/before	Refs
Wedge-shaped TiO_2 array	97 %	87 % (P25)	1.12	this work
TiO_2 by doping	63.3 %	70 %	0.90	S31
	0.65[#]	0.9	0.72	S32
	1.1	1.7	0.65	S33
	1.2	1.63	0.74	S34
	0.84	0.98	0.86	S35
TiO_2 by hydrogenation	0.93	0.95	0.98	S36
	0.68	0.68	1.00	S37
	1.52	1.48	1.03	S38
	97%	97%	1.00	S39

[#] the decimal data was not unified.

As the light absorption of TiO_2 in UV region was not unified in various references, the UV absorption ratio was used at 300 nm after and before TiO_2 modification (doping or hydrogenation), and summarized in Table S7. It was notable our wedge-shaped nanoarray increased the UV absorption compared with P25. Most doping or hydrogenation can red-shift the UV absorption edge of TiO_2 at the cost of decreasing UV absorption (0.65-0.98).

Table S8. Sizes of the simulation parameters for other three color samples in visible absorption

	P-TiO_2	**B-TiO_2**	**G-TiO_2**
width (w_1)	**30-40 nm**	**40-50 nm**	**60-70 nm**
width (w_2)	**180-200 nm**	**220-280 nm**	**300-350 nm**
length	**2.6 μm**	**2.8 μm**	**3.0 μm**
thickness (top)	**10-20 nm**	**10-20 nm**	**10-20 nm**
thickness (bottom)	**60-90 nm**	**60-90 nm**	**60-90 nm**

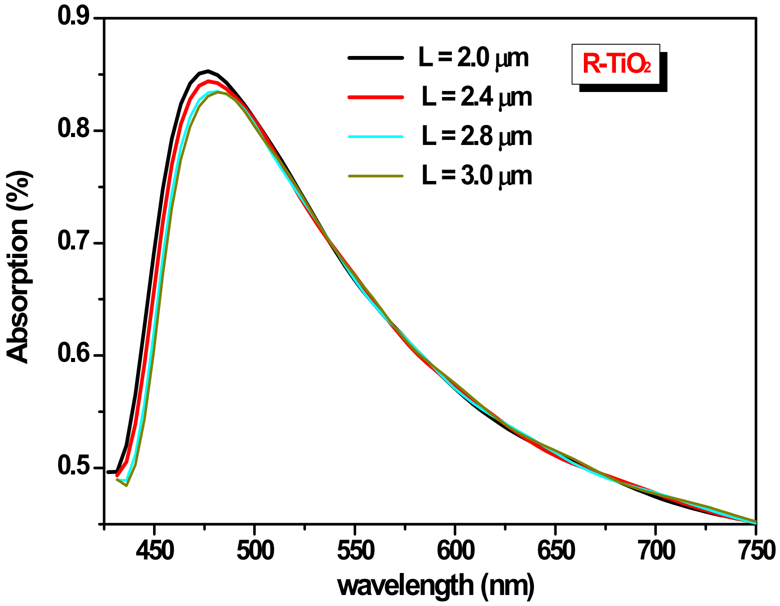

Fig. S24. FEM simulation of absorption spectra of R-TiO_2 (L = 2.4 μm) by changing the length from 2.0 to 3.0 μm with the same other parameters. It could be seen clearly that the shape and position of the peak had little influence by length (taking the red sample as an example).

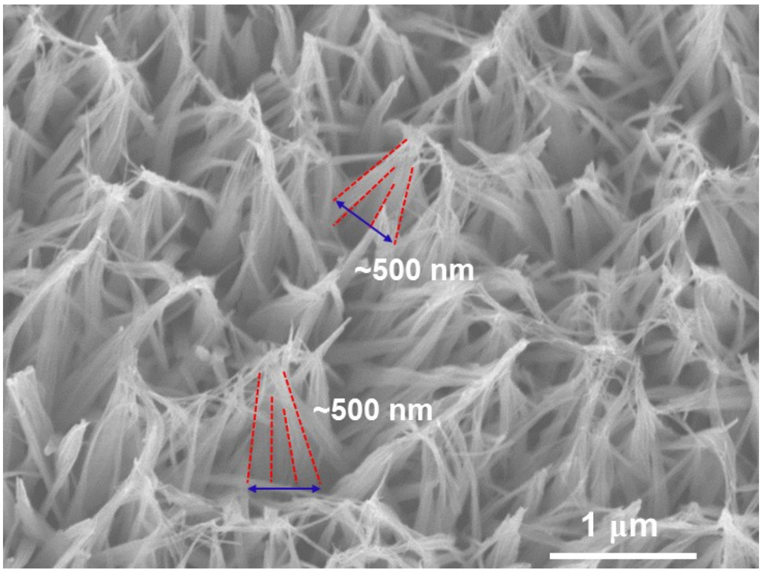

Fig. S25. SEM image of the R-TiO_2/TF taken from aggregated region. It could be seen that some nanosheets aggregated and formed bigger sizes (corresponding to the bigger size in Table S6). The wedge-like array was not uniform, which explained the influence on NIR absorption in FEM simulation.

References

S1 J. J. Fan, S. W. Liu, J. G. Yu, *J. Mater. Chem.*, 2012, **22**, 17027-17036.

S2 D. J. Yang, H. W. Liu, Z. F. Zheng, Y. Yuan, J. C. Zhao, E. R. Waclawik, X. B. Ke, H. Y. Zhu, *J. Am. Chem. Soc.* 2009, **131**, 17885-17893.

S3 I. Alessandri, *J. Am. Chem. Soc.* 2013, **135**, 5541-5544.

S4 D. W. Lynch, C. G. Olson, J. H. Weaver, *Phys. Rev. B* 1975, **11**, 3617-3624.

S5 X. Chen, S. S. Mao, *Chem. Rev.* 2007, **107**, 2891-2959.

S6 V. Aravindan, N. Shubha, Y. L. Cheah, R. Prasanth, M. Chuiling, R. R. Prabhakar, S. Madhavi, *J. Mater. Chem. A* 2013, **1**, 308-316.

S7 W. R. Zhao, M. Zhang, Z. Y. Ai, Y. N. Yang, H. P. Xi, Q. M. Shi, X. H. Xu, H. X. Shi, *J. Phys.Chem.C* 2014, **118**, 23117-23125.

S8 C. H. Wang, C. L. Shao, X. T. Zhang, Y. C. Liu, *Inorg. Chem.* 2009, **48**, 7261-7268.

S9 G. Sahasrabudhe, S. M. Rupich, J. Jhaveri, A. H. Berg, K. A. Nagamatsu, G. Man, Y. J. Chabal, A. Kahn, S. Wagner, J. C. Sturm, J. Schwartz, *J. Am. Chem. Soc.* 2015, **137**, 14842-14845.

S10 Z. Wang, C. Y. Yang, T. Q. Lin, H. Yin, P. Chen, D. Y. Wan, F. F. Xu, F. Q. Huang, J. H. Lin, X. M. Xie, M. H. Jiang, *Adv. Funct. Mater.* 2013, **23**, 5444-5450.

S11 S. SÖdergren, H. Siegbahn, *J. Phys. Chem. B* 1997,**101**, 3087-3090.

S12. Z. J. Sun, H. F. Zheng, J. S. Li, P. W. Du, *Energy Environ. Sci.*, 2015, **8**, 2668-2676.

S13. Y. Goto, K. Taniguchi, T. Omata, S. O. Y.Matsuo, N. Ohashi, S. Ueda, H. Yoshikawa, Y. Yamashita, H. Oohashi, K. Kobayashi, *Chem. Mater.,* 2008, **20**, 4156-4160.

S14. W. W. Lin, H. Y. Cheng, J. Ming, Y. C. Yu, F. Y. Zhao, *J. Catal.* 2012, **291**, 149-154.

S15 A. J. B. Dutra, G. P. Rocha, F. R. Pombo, *J. Hazard. Mater.* 2008, **152**, 648-655.

S16 A. D. M. Ferreira, M. Marchesiello, P. X. Thivel, *Sep. Purif. Technol.* 2013, **107**, 109-117.

S17 F. Akbal, S. Camcı, *Desalination* 2011, **269**, 214-222.

S18 I. Kabdaslı, T. Arslan, T. ö. Hanci, I. A. Alaton, O. Tünay, *J. Hazard. Mater.* 2009, **165**, 838-845.

S19 G. G. Bessegato, J. C. Cardoso, B. F. D. Silva, M. V. B. Zanoni, *Appl. Catal. B: Environ.* 2016, **131**, 161-168.

S20 N. S. Arul, D. Mangalaraj, R. Ramachandran, A. N. Grace, J. I. Han, *J. Mater. Chem. A*, 2015, **3**, 15248-15258.

S21 P. Salama, D. Berk, *Ind. Eng. Chem. Res.* 2005, **44**, 7071-7077.

S22 J. K. Yang, A. P. Davis, *Environ. Sci. Technol.* 2000, **34**, 3789-3795.

S23 J. K. Yang, A. P. Davis, *Environ. Sci. Technol.* 2000, **34**, 3796-3801.

S24 A. P. Davis, D. L. Green, *Environ. Sci. Technol.* 1999, **33**, 609-617.

S25 S. Satyro, R. Marotta, L. Clarizia, I. D. Somma, G. Vitiello, M. Dezotti, G. Pinto, R. F. Dantas, R. Andreozzi, *Chem. Eng. J.* 2014, **251**, 257-268.

S26 B. A. Labaran, M. S. Vohra, *Environ.Technol*. 2014, **35**, 1091-1100.

S27 A. F. Alkaim, T. A. Kandiel, F. H. Hussein, R. Dillert, D. W. Bahnemann, *Catal. Sci. Technol.* 2013, **3**, 3216–3222.

S28 X. Zhao, L. B. Guo, C. Z. Hu, H. J. Liu, J. H. Qu, *Appl. Catal. B: Environ.* 2014, **144**, 478-485.

S29 X. Zhao, L. B. Guo, J. H. Qu, *Chem. Eng. J.* 2014, **239**, 53-59.

S30 X. Zhao, L. B. Guo, B. F. Zhang, H. J. Liu, J. H. Qu, *Environ. Sci. Technol.* 2013, **47**, 4480-4488.

S31 R. Asahi, T. Morikawa, T. Ohwaki, K. Aoki, and Y. Taga, *Science*., 2001, **293**, 269-271.

S32 Y. W. Huang, Q. K. Shang, D. Wang, S. Yang, H. Y. Guan, Q. Lu, and S. H. Tsang, *Appl. Catal. B: Environ.*, 2016, **187**, 59-66.

S33 Y. B. Wang, Y. N. Zhang, G. H. Zhao, H. Y. Tian, H. J. Shi, and T. C. Zhou, *ACS Appl. Mater. Interfaces.*, 2012, **4**, 3965−3972.

S34 X. Chen, D. X. Zhao, K. W. Liu, C. R. Wang, L. Liu, B. H. Li, Z. Z. Zhang, and D. Z. Shen, *ACS Appl. Mater. Interfaces.*, 2015, **7**, 16070−16077.

S35 Z. H. Shah, J. S. Wang, Y. Z. Ge, C. Wang, W. X. Mao, S. F. Zhang, and R. W. Lu, *J. Mater. Chem. A,*

2015, **3**, 3568–3575.

S36 Z. Wang, C. Y. Yang, T. Q. Lin, H. Yin, P. Chen, D. Y. Wan, F. F. Xu, F. Q. Huang, J. H. Lin, X. M. Xie, and M. H. Jiang, *Energy Environ. Sci.*, 2013, **6**, 3007-3014.

S37 T. Q. Lin, C. Y. Yang, Z. Wang, H. Yin, X. J. Lu, F. Q. Huang, J. H. Lin, X. M. Xie, and M. H. Jiang, *Energy Environ. Sci.*, 2014, **7**, 967-972.

S38 J. X. Qiu, S. Li, E. Gray, H. W. Liu, Q. F. Gu, C. H. Sun, C. Lai, H. J. Zhao, and S. Q. Zhang, *J. Phys. Chem. C*, 2014, **118**, 8824-8830.

S39 N. Liu, C. Schneider, D. Freitag, M. Hartmann, U. Venkatesan, J. Müller, E. Spiecker, P. Schmuki, *Nano Lett*. 2014, **14**, 3309-3313.